Supplementary Material

Superior electromagnetic interference shielding 3D graphene nanoplatelets/reduced graphene oxide foam/epoxy nanocomposites with high thermal conductivities

Chaobo Liang[a#], Hua Qiu[a#], Yangyang Han[a], Hongbo Gu[c]*, Ping Song[a], Lei Wang[a], Jie Kong[a], Dapeng Cao[d]*, Junwei Gu[a, b]*

[a] MOE Key Laboratory of Material Physics and Chemistry under Extraordinary Conditions, Shaanxi Key Laboratory of Macromolecular Science and Technology, Department of Applied Chemistry, School of Science, Northwestern Polytechnical University, Xi' an, Shaanxi, 710072, P.R. China.

[b] Institute of Intelligence Material and Structure, Unmanned System Research Institute, Northwestern Polytechnical University, Xi'an, Shaanxi, 710072, P.R. China.

[c] Shanghai Key Lab of Chemical Assessment and Sustainability, School of Chemical Science and Engineering, Tongji University, Shanghai 200092, P.R. China.

[d] State Key Lab of Organic-Inorganic Composites, Beijing University of Chemical Technology, Beijing 100029, P.R. China

Corresponding Authors: gjw@nwpu.edu.cn & nwpugjw@163.com (J. Gu); hongbogu2014@tongji.edu.cn (H. Gu); caodp@mail.buct.edu.cn (D. Cao)

[#]The authors Chaobo Liang[#] and Hua Qiu[#] contributed equally to this work and should be considered *co*-first authors.

S1 Experimental Section

S1.1 Materials

Bisphenol F epoxy of Epon 862 and curing agent of EK3402 were both purchased from Hexion Inc (America), and the corresponding chemical structures are shown in Fig. S1. Graphite nanoplatelets (GNPs, KNG-180), with diameter of 40 um and super diameter/thickness ratio of 250, were received from Xiamen Knano Graphene Technology Co. Ltd. (Fujian, China). Graphite flake (325 mesh, 99.8%) was provided by Alfa Aesar Co. Ltd. (China). Potassium persulfate ($K_2S_2O_8$, ≥99%), phosphorus pentoxide (P_2O_5, ≥98%), potassium permanganate ($KMnO_4$, ≥99%), sulfuric acid (H_2SO_4, 98%), hydrochloric acid (HCl, 37 wt%) and hydrogen peroxide (H_2O_2, 30 wt%) were all purchased from Beijing Chemical Factory (Beijing, China). Poly (vinyl alcohol) (PVA, weight-averaged molecular weight ～205,000, 99% hydrolyzed) was supplied by Aladdin Reagent Co., Ltd. (Shanghai, China).

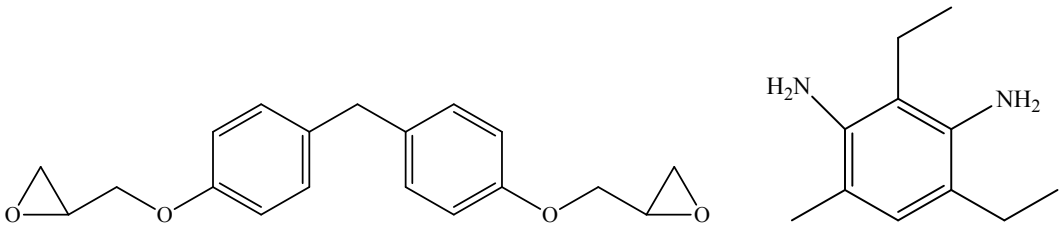

Epon 862 EK3402

Fig. S1 Chemical structure of Epon 862 and EK3402.

S1.2 Characterizations

Fourier transform infrared (FTIR) spectra of the samples were obtained on a Bruker Tensor 27 equipment (Bruker Corp., Germany). X-ray photoelectron spectroscopy (XPS) analyses of the samples were carried out using PHI5400 equipment (PE Corp., England). Thermal gravimetric analysis (TGA) of the samples were conducted by STA 449F3 equipment (NETZSCH Corp., Germany) at 10 $^oC\ min^{-1}$ at air atmosphere. Scanning electron microscope (SEM) morphologies of the samples were analyzed by

VEGA3-LMH equipment (TESCAN Corporation, Czech Republic). Thermally conductive coefficient (λ) and thermal diffusivity (α) values of the samples were measured using a TPS2200 Hot Disk instrument (AB Corp., Sweden) by the transient plane source method according to standard ISO 22007-2:2008. The thermal images of the samples were taken by a infrared thermal imager of Ti 300 equipment (Fluke Corp., America), placing the samples on a hot plate (Linkam GS315) at a constant temperature 90 ^{o}C. The electrical conductivity of the samples was measured using a RTS-8 Four Probe instrument (Guangzhou Four Probe Technology Corp., China). The characteristic EMI shielding parameters of the samples were tested by MS4644A Vector Network Analyzer instrument (Anritsu Corp., Japan) using the wave-guide method at the X-band frequency range according to ASTM D5568-08, and the corresponding dimension of the samples with length of 22.86 mm, width of 10.16 mm, and thickness of 3 mm. The indentation experiment was performed with an using a G200 nanoindenter (Agilent Corp., America). The peak indentation load was set as 9 mN with the fixed loading and unloading rates of 300 and 450 mN/s, respectively.

S2. Element content and C/O atomic ratio of the GO, GO/PVA and rGO/PVA

Table S1 Element content and C/O atomic ratio of GO, GO/PVA and rGO/PVA

Samples	Element content / %		C/O atomic ratio
	C	O	
GO	72.2	27.8	2.6
GO/PVA	72.1	27.9	2.6
rGO/PVA	91.8	8.2	11.2

S3. Morphology of 3D GNPs/rGO foam

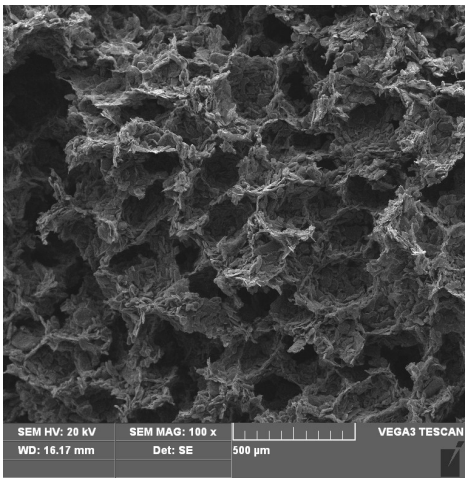

Fig. S2 SEM image of 3D GNPs/rGO foam

S4. Porosity of 3D GNPs/rGO foam

Table S2. The porosity of 3D GNPs/rGO foam

GNPs content (wt%)	7.9	14.6	20.4
Porosity (%)	95.7	91.8	88.2

$$P = \frac{V_0 - V}{V_0} \times 100\% = \left(1 - \frac{\rho_0}{\rho}\right) \times 100\% \quad \text{(S1)}$$

where P is the material porosity, %; V_0 is the volume of the material in its natural state, or apparent volume, cm^3 or m^3; ρ_0 is the bulk density of the material, g/cm^3 or kg/m^3; V is the absolute compact volume of the material, cm^3 or m^3; ρ is the material density, g/cm^3 or kg/m^3.

S5. The anisotropy thermal conductivity and theoretical values from correlative models of 3D GNPs/rGO/EP nanocomposites

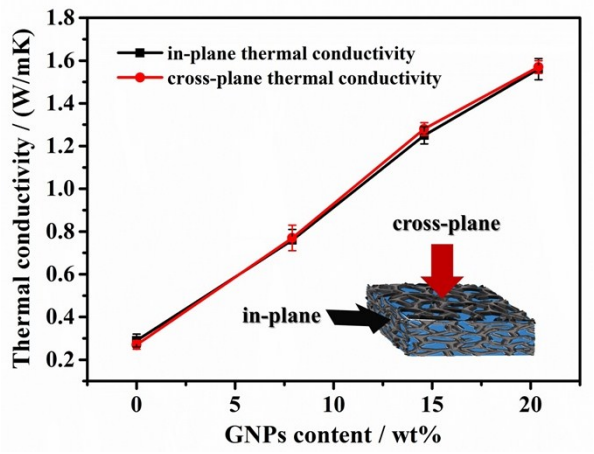

Fig. S3 Thermal conductivity of 3D GNPs/rGO/EP nanocomposites

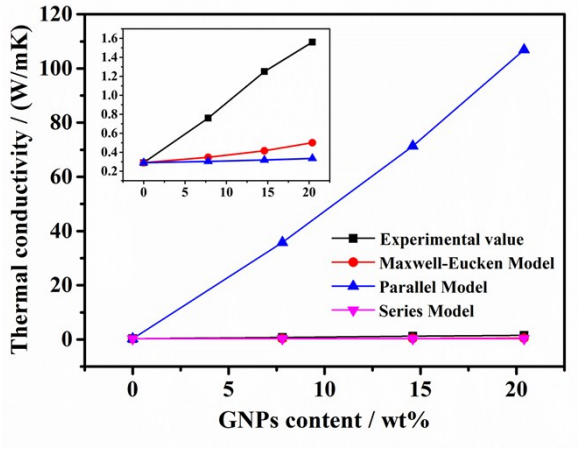

Fig. S4 Experimentally and theoretical l values from correlative models of 3D GNPs/rGO/EP nanocomposites.

S6. Electromagnetic shielding effectiveness: theory and measurement

MI SE of a material is defined by the amount of reduction in the incident radiation intensity after passing through a material, the total EMI SE (SE_T) of a material consists of the contributions fromis the sum of the reflection (SE_R), absorption (SE_A) and multiple reflections (SE_M), given by eqn (S1) [1]

$$SE_T = SE_A + SE_R + SE_M \quad (S2)$$

In a vector network analyzer, S_{11} represents reflection coefficient, S_{12} represents transmission coefficient, S_{21} represents back ward transmission coefficient and S_{22}

represents reverse reflection coefficient. The SE_T is evaluated from the S parameters by using the following eqn [2]

$$SE_T\,(dB) = -10\log\left(S_{12}^2\right) = -10\log\left(S_{21}^2\right) = -10\log(T) \quad \text{(S3)}$$

$$SE_R\,(dB) = -10\log\left(1 - S_{11}^2\right) = -10\log(1 - R) \quad \text{(S4)}$$

$$SE_A\,(dB) = -10\log\left(\frac{S_{12}^2}{1 - S_{11}^2}\right) = -10\log\left(\frac{T}{1 - R}\right) \quad \text{(S5)}$$

Here, $T = S_{12}^2 = S_{21}^2$ and $R = S_{11}^2$.

The dependence of SE_R and SE_A on complex permittivity and permeability are given by

$$SE_A\,(dB) = 20\frac{d}{\delta}\log e = 20d\sqrt{\frac{\mu_r \omega \sigma_s}{2}}\log e \quad \text{(S6)}$$

$$SE_R\,(dB) = 10\log\left(\frac{\sigma_s}{16\mu_r \omega \varepsilon_0}\right) \quad \text{(S7)}$$

where d is the thickness of the shield, μ_r is the relative magnetic permeability, δ is the skin depth, $\sigma_s = \omega\varepsilon_0\varepsilon''$ is the frequency dependent conductivity, ε'' is the maginary part of permittivity (dielectric loss factor), ω is the angular frequency ($\omega = 2\pi f$) and ε_0 is the permittivity of the free space.

S7. Thermal properties of the EP nanocomposites

Fig. S2 shows the TGA profiles of the rGO/EP and 3D GNPs/rGO/EP nanocomposites in the air atmosphere. The corresponding thermal parameters obtained from TGA curves are summarized in Table S2.

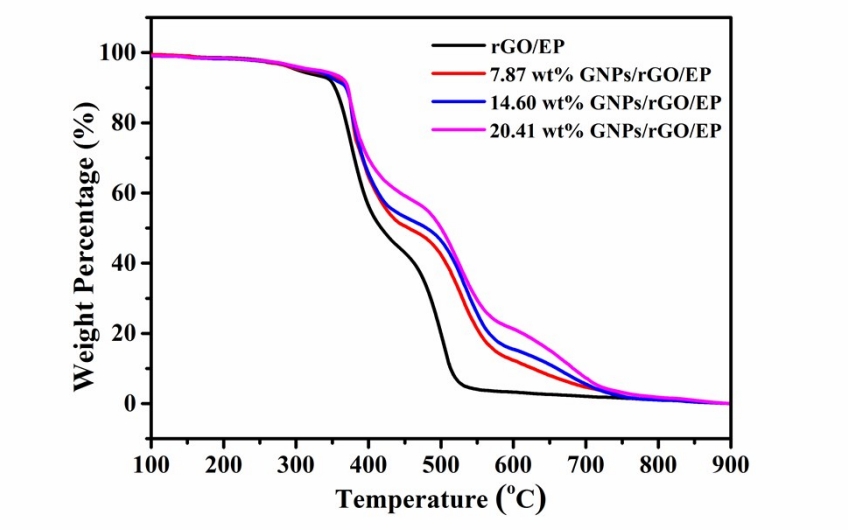

Fig. S5 TGA curves of the rGO/EP and 3D GNPs/rGO/EP nanocomposites.

Table S3 Thermal parameters of the rGO/EP and 3D GNPs/rGO/EP nanocomposites

Samples	Weight loss temperature (°C)		T_{HRI} (°C)
	T_5	T_{30}	
rGO/EP	303	380	171.1
7.9 wt% GNPs/rGO/EP	313	391	176.3
14.6 wt% GNPs/rGO/EP	320	392	178.0
20.4 wt% GNPs/rGO/EP	330	399	182.0

The sample's heat-resistance index [3, 4] is calculated by Eq. (1).

$T_{Heat\text{-}resistance\ index}=0.49\times[T_5+0.6\times(T_{30}-T_5)]$ (Eq. (1)). T_5 and T_{30} is corresponding decomposition temperature of 5% and 30% weight loss, respectively.

It is observed that the thermal decomposition of the rGO/EP and 3D GNPs/rGO/EP nanocomposites happens in two stages, as reported in the literature.[5, 6] The first one from 350 to 400 °C is due to the breakdown of EP network and the second one from 450 to 600 °C is attributed to the degradation of benzene rings in the EP polymer backbone. Meantime, with the addtion of GNPs, the first decomposition temperature

(T_5, 5 wt% weight loss) for the 3D GNPs/rGO/EP nanocomposites with 7.9 wt% GNPs increases up to 27 °C and the second decomposition temperature (T_{30}, 30 wt% weight loss) increases up to 19 °C relative to the rGO/EP nanocomposites. And the corresponding T_{HRI} is increased obviously (from 176.3 °C for GNPs/rGO/EP nanocomposites with 7.9 wt% GNPs to 182.0 °C for GNPs/rGO/EP nanocomposites with 20.4 wt% GNPs), compared to that of rGO/EP nanocomposites (171.1 °C). This confirms that the 3D scaffolds can improve the interfacial compatibility between GNPs and EP matrix, leading to an enhanced thermal stability of the 3D GNPs/rGO/EP nanocomposites.[7]

S8. Mass density measurements and comparisons of 3D GNPs/rGO/EP nanocomposites

Table S4 Comparison of theoretical and measured mass of epoxy.

	V (cm3)	m_0 (g)	□$_0$ (g/cm^3)	□ (g/cm^3)	m (g)	$m_{measure}$ (g)
7.9 wt% GNPs/rGO/EP	30	3.15	2.25	1.17	33.46	33.34
14.6 wt% GNPs/rGO/EP	30	6.15	2.25	1.17	31.90	31.76
20.4 wt% GNPs/rGO/EP	30	9.15	2.25	1.17	30.34	30.10

$$m = \left(V - \frac{m_0}{\rho_0} \right) \times \rho \tag{S8}$$

where $m_{measure}$ is the measured mass of epoxy, g; m is the theoretical mass of epoxy, g; V is the volume of the GNPs/rGO foam in its natural state, cm^3; m_0 is the mass of the GNPs/rGO foam, g; ρ_0 is the density of the GNPs/rGO, g/cm^3; ρ is the density of epoxy, g/cm^3.

References

1. N. Colaneri, L. Shacklette, *IEEE T. Instrum. Meas.*, 1992, **41**, 291-297.
2. Y. Yang, M. Gupta, *Nano Lett.*, 2005, **5**, 2131-2134.
3. J. Gu, S. Xu, Q. Zhuang, Y. Tang, J. Kong, *IEEE T. Dielect. El. In.*, 2017, **24**, 784-790.
4. L. Tang, J. Dang, M. He, J. Li, J. Kong, Y. Tang and J. Gu, *Compos. Sci. Technol.*, 2019, **169**, 120-126.
5. H. Gu, J. Guo, Q. He, S. Tadakamalla, X. Zhang, X. Yan, Y. Huang, H. Colorado, S. Wei, Z. Guo, *Ind. Eng. Chem. Res.*, 2013, **52**, 7718-7728.
6. H. Gu, H. Zhang, J. Lin, Q. Shao, D. Young, L. Sun, T. Shen and Z. Guo, *Polymer*, 2018, **143**, 324-330.
7. J. Lin, Z. Lin, Y. Pan, C. Hsieh, C. Huang, C. Lou, *J. Appl. Polym. Sci.*, 2016, **133**, 43474.